



# The deposition of Group 6A-derived inorganic semiconductor films as studied by quartz crystal microgravimetry

N. Myung <sup>a,\*</sup>, S. Kim <sup>a</sup>, D. Lincot <sup>b</sup>, C. Lepiller <sup>b</sup>, N.R. de Tacconi <sup>c</sup>,  
K. Rajeshwar <sup>c,1</sup>

<sup>a</sup> Department of Applied Chemistry, Konkuk University Chungju Campus, Chungju, Chungbuk 380-701, South Korea

<sup>b</sup> Laboratoire d'Electrochimie et de Chimie Analytique (CNRS), Ecole Nationale Supérieure de Chimie de Paris,  
11 rue Pierre et Marie Curie, 75 231 Paris Cedex 5, France

<sup>c</sup> Department of Chemistry and Biochemistry, The University of Texas at Arlington, Arlington, TX 76019-0065, USA

Received 2 August 1999; received in revised form 1 October 1999

## Abstract

This paper focuses on the use of QCM for the study of semiconductor film deposition processes. Specifically the electro-synthesis of metal chalcogenides ( $\text{In}_2\text{S}_3$ , CdS, and CdTe) is considered. A brief background is first given for electrodeposition as a process candidate for semiconductor film preparation. Previous studies are reviewed on the use of QCM (and specifically EQCM) in this area. New combined voltammetry-EQCM data are presented for the oxidative deposition of sulfur on polycrystalline Au surfaces from alkaline sulfide baths. The anodic growth of CdS films and the cathodic electro-synthesis of  $\text{In}_2\text{S}_3$  are studied by the combined approach. Finally, data are presented on the cathodic electro-synthesis of CdTe films using EQCM in a rotating disc electrode (RDE) configuration. From an instrumental perspective, the presented data illustrate the virtues of combining the QCM technique with cyclic voltammetry, coulometry, and hydrodynamic (RDE) voltammetry for studies of semiconductor film deposition. © 2000 Elsevier Science Ltd. All rights reserved.

**Keywords:** Quartz crystal microgravimetry; Semiconductor film deposition processes; Electro-synthesis; Metal chalcogenides

## 1. Introduction

As also exemplified by the other articles in this Special Issue, quartz crystal microgravimetry (QCM) has been successfully used in the study of many electrochemical problems, including trace analysis; mass transport in redox and conducting polymers; double layer properties and depletion layer effects at electrode/solution interfaces; surface roughness and liquid properties;

adlayers and surface reconstruction; and kinetics of electrochemical processes. The early observation of Sauerbrey [1] that changes in the resonant frequency of a piezoelectric crystal such as quartz are proportional to mass changes, led logically to the extensive use of the electrochemical QCM (EQCM) counterpart for metal deposition and stripping analyses [2–4]. Many similar studies were also performed on the electrodeposition (and electro-dissolution) of conducting polymer films [5]. However, instances where QCM or EQCM has been utilized for the study of inorganic semiconductor films are more scarce. This topic, therefore, constitutes the focus of this paper.

\* Corresponding author.

<sup>1</sup> Also corresponding author.

Semiconductor films derived from Group 6A (16) elements (O, S, Se, Te) have applicability in many optoelectronic devices ranging from solar cells to xerographic systems. Depending on their chemical composition and stoichiometry, these materials exhibit interesting optoelectronic properties, including photoconductivity and both n- and p-type semiconductor behavior. Specific examples of binary and ternary compounds include CdS, ZnO, CdTe, CdSe, CuInSe<sub>2</sub>, etc.

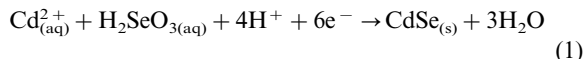
### 1.1. Preparation of thin films

Many electronic and optoelectronic applications necessitate the deposition of the aforementioned materials in thin film form on targeted substrates. High temperature (e.g. evaporation) and ultra-high vacuum (e.g. sputtering) methods have been extensively employed for the preparation of semiconductor thin films. Indeed, QCM has served a useful function in many of these cases as a film thickness monitor of the gas phase deposition process. However, low-temperature film deposition approaches have many attractive features. For example, problems associated with interlayer diffusion and preferential evaporation that plague high-temperature deposition processes are absent here. Electrodeposition [6,7] and chemical bath deposition (CBD) [8,9] are the two major process candidates for low-temperature film deposition approaches. Both these processes are low cost and readily amenable to scale-up. Relative to electrodeposition, CBD does offer the advantage of not requiring a conductive substrate. On the other hand, electrodeposition, because of its electrical nature, offers precise process control. Both processes are compatible with irregular substrate shapes.

### 1.2. Film deposition chemistry and electrochemistry

Electrodeposition of metal oxide/chalcogenide films can be done either anodically or cathodically [10]. In the former approach, a metal anode is exposed to an alkaline medium containing X<sup>2-</sup> precursor species (X = O, S, Se, Te). The main difficulty with anodic film growth is that associated with mass transport limitations. That is, sustained film growth necessitates the flux of metal ions 'outward' to the solution boundary and/or X<sup>2-</sup> species 'inward' toward the metal/film boundary. Thus, the (growing) semiconductor film presents a barrier to film growth that ultimately becomes self-limiting.

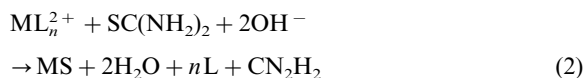
In the cathodic approach, soluble precursor species are co-deposited onto a suitable (inert) substrate such as conductive glass, glassy carbon, gold, etc. This is exemplified by the overall reaction scheme for the deposition of CdSe:



Variants of this cathodic scheme have been developed, including the use of non-aqueous deposition baths [10]. Another innovation begins with the initial deposition of a chalcogen (e.g. sulfur) multilayer on a gold substrate followed by cathodic reduction of this layer to increase the chalcogenide ion activity at the electrode/solution interface. Subsequent dosing of the bath with the requisite metal ions generates an insoluble metal chalcogenide layer at the substrate/solution interface. This approach has been demonstrated for iron sulfide [11], indium sulfide [12], and cadmium selenide [13]. Further data are presented below.

Interestingly, metal oxide films can also be electrodeposited cathodically using soluble precursor species. Two categories of cathodic oxide deposition processes can be recognized. The first (as in the anodic approach above) involves a change in the oxidation state, as exemplified by the cathodic electrosynthesis of Cu<sub>2</sub>O from Cu(II) precursor species [14]. The second category is not based on a change of the metal oxidation state but on an electrochemical reaction involving oxygen or other additives (e.g. nitrate). The net effect is electrochemical generation of OH<sup>-</sup> ions and subsequent precipitation of the oxide/hydroxide phase [15–18].

The CBD process can be illustrated by the classical scheme for deposition of metal sulfide (MS) films [9]:



where L is a ligand for the metal ion. Sulfide compounds are by far the most studied category under CBD but an increasing number of metal selenides have been synthesized as well [9]. Other than thiourea (see Eq. (2) above), many chalcogenide precursors have been used; these have been reviewed recently [8,9].

### 1.3. Prior studies of inorganic semiconductor film deposition by QCM

Table 1 contains a listing of studies where QCM (or EQCM) has been employed in studies of inorganic semiconductor film deposition. The scope of this technique is enhanced when combined with other electrochemical probes such as cyclic voltammetry and coulometry. Of course this feature is common to other test systems (e.g. metals, conducting polymers) as well. Nonetheless, chalcogenide film deposition involves electrochemical reaction steps intertwined with chemical processes that are much easier to interpret with a combined approach. We illustrated this notion with data on Te many years ago [19].

More recently, EQCM has been used in conjunction with coulometry to probe changes in film stoichiometry

Table 1  
Examples of the use of QCM (or EQCM) in studies of inorganic semiconductor film deposition

Entry no.	System(s) studied <sup>a</sup>	Ref. no(s).
1	Te	[19]
2	Cd–Se	[13,20–22]
3	Cd–Te	[23]
4	Cu–S, Cu–In–S	[24,25]
5	Cu–Se	[26]
6	Fe–S	[11]
7	In–S	[12]
8	Zn–O	[16]
9	Cu–O	[27]
10	Cd–S (CBD)	[28,29]
11	Zn–S (CBD)	[30]
12	Cd–Se (CBD)	[31]
13	Se	[32]

<sup>a</sup> Films were deposited electrochemically in all cases unless otherwise indicated in parentheses.

in the Cu–S system [24] with increasing anodization and  $\text{In}^{3+}$  insertion dynamics in the ternary Cu–In–S system [25]. A rotating microbalance has been designed to combine the virtues of a rotating disk electrode configuration with the QCM probe and used for the study of the Cu–Se binary system [26]. The EQCM technique has been applied to the study of Cu/Cu<sub>2</sub>O layered nanostructures [27]. Flow injection has been combined with EQCM for the study of CdSe film deposition [22]. The use of a dual electrochemical cell with selective stripping and EQCM analyses, has facilitated the compositional assay of metal chalcogenide films [20,21,23]. Finally, QCM has been combined with AC impedance spectroscopy for the study of CBD of CdS [28]. Comparison of the temporal derivative,  $dm/dt$

(obtained from QCM) with predictions from nucleation/growth models (usually elaborated with the aid of chronoamperometric experiments) provides new mechanistic insights into the film growth process itself [9,28,33].

## 2. Experimental

Details of the electrochemical instrumentation and the EQCM set-up are given elsewhere [22,26,34]. Either a 5 or a 9 MHz gold-overlaid AT-cut quartz crystal was used as the mass sensor and as the working electrode. All potentials herein are quoted with respect to either Ag/AgCl/3 M KCl (or 3 M NaCl) or SCE reference. All chemicals were from commercial sources and were of the highest purity available; they were used as received. Deaerated (ultrapure N<sub>2</sub> or argon purged) and double-distilled water was used in all the experiments. All data below pertain to the laboratory ambient temperature unless otherwise noted.

Experiments on CdTe deposition were carried out at 70–80°C using a custom-made rotating EQCM setup. The solution was made of dissolved cadmium sulfate (0.5 M) and tellurium dioxide ( $10^{-3}$  M) at pH 1.4.

## 3. Results and discussion

### 3.1. Surface modification of gold with sulfur

Oxidative deposition of sulfur on gold has been studied by previous authors (including one of us, N.R. de T) using in situ spectroscopy and/or voltammetry [35–38]. Since this process is an important component of both the anodic deposition of metal chalcogenides and the cathodic electrosynthesis of these compounds, we present below new data on the study of sulfur deposition on gold by combined voltammetry-EQCM.

Fig. 1 contains a cyclic voltammogram (Fig. 1a) and an accompanying EQCM trace (Fig. 1b) for an initially bare polycrystalline gold surface in a 1 M NaOH/10 mM Na<sub>2</sub>S electrolyte. The potential scan was initiated in the positive direction from ca. –1.5 V. The barely discernible anodic voltammetric feature at  $\approx -0.90$  V is accompanied by mass gain that can be identified as the oxidative underpotential deposition of sulfur. This process has been shown by other authors [38] to correspond to a fractional monolayer of sulfur on the gold surface. Further negative potential excursion culminates in a prominent anodic wave peaking at  $\approx -0.2$  V with accompanying mass gain. This corresponds to multilayer deposition of sulfur. There is a slight mass loss at the tail of this peak corresponding to a weaker anodic feature at  $\approx 0$  V.

Sulfur deposition continues on the return cycle as manifest in the EQCM trace in Fig. 1b up to  $\approx -0.6$

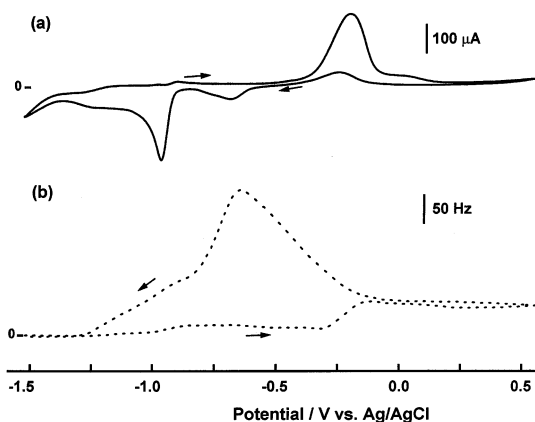


Fig. 1. Combined cyclic voltammetry (Fig. 1a) and EQCM (Fig. 1b) profiles for a polycrystalline Au surface in 1 M NaOH/10 mM Na<sub>2</sub>S. Each scan began at –1.5 V in the positive direction. The potential scan rate was 100 mV/s.

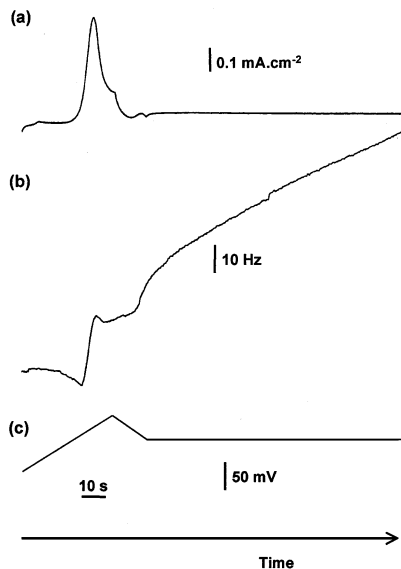


Fig. 2. Voltammetry (Fig. 2a), EQCM (Fig. 2b), and potential waveform (Fig. 2c) for the oxidative deposition of sulfur on the Au surface. The electrolyte was  $0.05 \text{ M Na}_2\text{S}/0.1 \text{ M Na}_2\text{SO}_4$ . The combined potentiodynamic/potentiostatic experiment began at  $-0.9 \text{ V}$ , then scanned in the positive direction up to  $0 \text{ V}$ ; the scan direction was switched at this point and a cathodic scan initiated to  $-0.22 \text{ V}$ . The potential was held at  $-0.22 \text{ V}$  for 2 min. The potential scan-rate was  $20 \text{ mV/s}$ .

V. Subsequently two cathodic features are accompanied by mass loss corresponding to the electro-reduction of the deposited sulfur layer. Soluble sulfide and polysulfide species are produced by this process and can be utilized for the deposition of metal sulfides as shown in the next section below. The ‘minimum’ in the EQCM trace (Fig. 1b) and the termination of the anodic wave on the return cycle (Fig. 1a) appear to coincide very

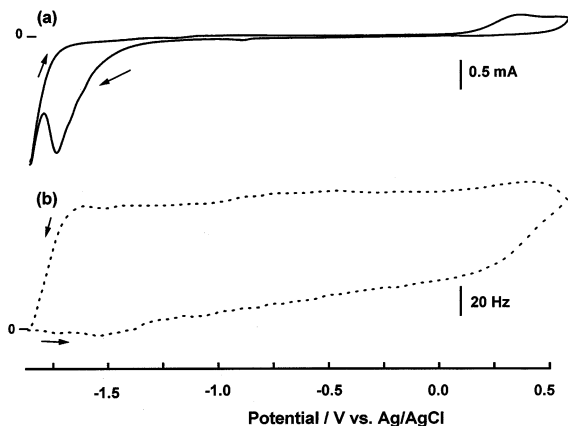


Fig. 3. Cyclic voltammetry (Fig. 3a) and EQCM (Fig. 3b) profiles for a Cd layer pre-deposited on the Au surface (see text). The electrolyte and scan conditions were as in Fig. 1.

well with the original rest potential of the medium ( $-0.6 \text{ V}$ ).

The sulfur deposition process is further amplified in the data in Fig. 2. A combined potentiodynamic-potentiostatic waveform was impressed on the current-mass measurements. Starting from a potential of  $-0.9 \text{ V}$ , the gold electrode was anodically scanned up to  $0 \text{ V}$ . The potential was then switched and arrested at  $-0.22 \text{ V}$  for a period of 2 min. A similar protocol was employed for metal sulfide film growth (see below).

### 3.2. Electrosynthesis of metal sulfide films on gold

One can either start with a metal layer on the native gold surface and anodically grow a sulfide film on it [7,36] or, alternatively as we have shown more recently [11,12], begin with a sulfur layer on the gold and cathodically grow a metal sulfide film on it. Both these complementary approaches are illustrated by combined voltammetry-EQCM data in this section.

Fig. 3 contains data pertaining to the classical anodic deposition approach for CdS [39–46]. A cadmium layer was initially deposited on the gold surface from a  $10 \text{ mM CdSO}_4/0.5 \text{ M Na}_2\text{SO}_4$  medium as described elsewhere [22]. Starting at a potential of  $-1.8 \text{ V}$ , this electrode was then scanned in the positive direction in a  $1 \text{ M NaOH}/10 \text{ mM Na}_2\text{S}$  medium. The corresponding voltammetry and EQCM profiles are contained in Fig. 3a and b, respectively. The initial mass gain at potentials between  $\approx -1.5$  and  $-1.1 \text{ V}$  corresponds to the growth of a few monolayers of CdS on the gold surface. The accompanying voltammogram features are barely discernible in Fig. 3a (at the current sensitivity shown) although we and others [40] have observed a sharp anodic feature at more sensitive scale settings.

A more gradual mass (Fig. 3b) increase, at potentials positive of  $-1.1$  up to  $\approx 0.2 \text{ V}$ , is accompanied by a region in the corresponding voltammetry profile in which there is very little current flow. This ca.  $1.3 \text{ V}$  voltage span corresponds to the ‘passivation regime’ in CdS film growth [40,41,45]. At potentials higher than  $\approx 0.2 \text{ V}$ , the mass uptake rate abruptly increases (Fig. 3b) accompanied by an anodic wave in Fig. 3a. On the return cycle, the mass continues to increase up to  $\approx 0.2 \text{ V}$  followed by minor changes that culminate in a pronounced mass loss at  $\approx -1.7 \text{ V}$ . The sulfur in CdS presumably is cathodically stripped leaving behind the residual Cd layer on the gold surface at  $-1.8 \text{ V}$ . This latter process is accompanied by a cathodic feature in the voltammogram at  $\approx -1.7 \text{ V}$  in Fig. 3a.

The new combined voltammetry-EQCM data on the anodic Cd–S system (presented in Fig. 3) is in good accord with the mechanistic picture gained earlier from voltammetric investigations [40,41]. Following the initial formation of a CdS adlayer of monomolecular dimensions, a barrier layer grows to  $\approx 50 \text{ \AA}$  thickness

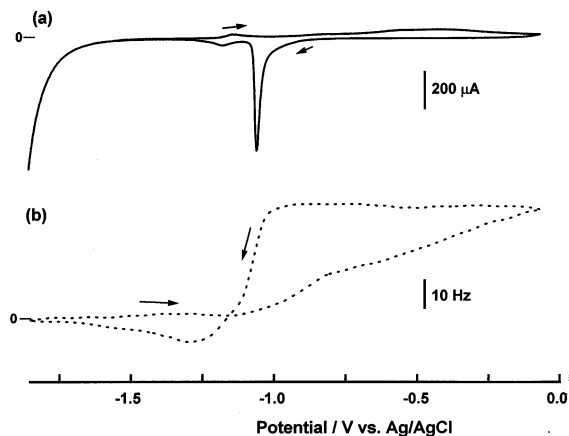


Fig. 4. As in Fig. 3 but for a 1 M NaOH electrolyte instead.

over a very wide potential span. This initial layer has been shown to be compact and uniform [40,41]. Subsequently, the kinetics abruptly change and a thick, porous layer grows on top of the initial film — this is the process seen in Fig. 3 beginning at  $\approx 0.2$  V.

It is worth noting that none of the features in Fig. 3 correspond to parallel oxide/hydroxide phase formation involving Cd. This can be assessed from a comparison of the voltammetry-EQCM profiles obtained for a Cd film in 1 M NaOH (i.e. in the absence of sulfide species) (Fig. 4). The mass uptake pattern on the forward scan in the two cases is clearly different (c.f. Fig. 3b and Fig.

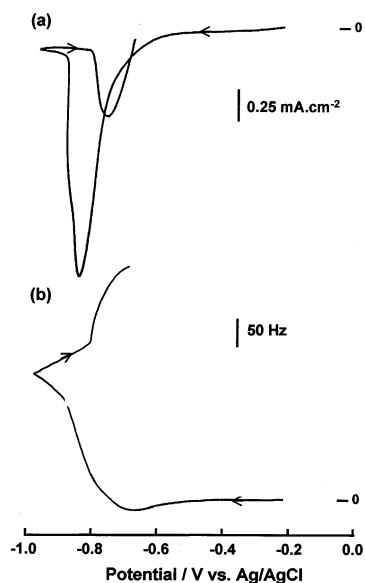


Fig. 5. Cyclic voltammetry (Fig. 5a) and EQCM (Fig. 5b) profiles for the cathodic deposition of  $\text{In}_2\text{S}_3$  and indium on a sulfur-modified Au surface (see Fig. 2). The solution was 0.01 M  $\text{In}_2(\text{SO}_4)_3$  acidified to pH  $\approx 2$  with HCl. The potential scan-rate was 20 mV/s.

4b) and the stripping of the cadmium oxide (formed on the forward scan) manifests as a sharp cathodic peak with accompanying mass loss at  $\approx -1.0$  V (Fig. 4). Indeed, examination of the EQCM profile provides a sensitive in situ indicator of the extent to which the metal sulfide film is contaminated by metal oxide/hydroxide phases. Voltammetry alone would be insensitive in this regard.

As mentioned earlier, an alternate metal sulfide growth strategy is to start with an initial sulfur layer on the gold surface built up as shown in Fig. 2. This is illustrated in Fig. 5. After the sulfur layer is grown on the Au surface to a requisite thickness (Fig. 2), the electrode is transferred (under potential control at  $-0.22$  V) to an  $\text{In}^{3+}$ -ion containing medium. Further scan in the negative direction results in the reductive deposition of indium (as the sulfide) with concomitant mass gain as illustrated in Fig. 5b. The initial mass loss seen at  $\approx -0.6$  V can be assigned to the nascent reduction of sulfur (as soluble sulfide species, Fig. 1). Subsequent precipitation of these species as indium sulfide result in the rapid mass gain seen after this initial feature (Fig. 5b).

Fig. 6 contains more voltammetry data on the In-S system illustrating the influence of thickness of the initial sulfur layer on subsequent assimilation. In Figs. 6a, b and c, the sulfur layers were grown potentiostatically (at  $-0.22$  V, Fig. 2) until they were approximately 15, 30, and 50 monolayers thick. The cathodic stripping peaks are shown in each case in Figs. 6a, b and c, respectively. When these sulfur layers are transferred (under potential control) to a HCl medium (pH  $\approx 2$ ) containing 0.01 M  $\text{In}_2(\text{SO}_4)_3$  and scanned in the negative direction as before, the stripping pattern is drastically altered as seen in Figs. 6a<sub>1</sub>, b<sub>1</sub> and c<sub>1</sub>. The cathodic feature at more negative potentials (seen especially in Figs. 6b<sub>1</sub> and c<sub>1</sub>) presumably corresponds to proton reduction.

Finally, referring back to Fig. 5, the subsequent mass gain and the cathodic wave at  $\approx -0.75$  V seen on the reverse scan (after switching the scan direction at  $-1.0$  V) have been discussed earlier [12]. These features arise from the deposition of indium atop the  $\text{In}_2\text{S}_3$  layer. Interestingly, this deposition is catalyzed by the indium sulfide layer; no deposition of indium is seen at these potentials when the sulfide layer is absent on the gold surface.

### 3.3. Electrodeposition of CdTe

Since the pioneering work by Kröger et al. [47,48] on binary II–VI and III–V semiconductor compounds, CdTe represents the most widely studied and a model system for semiconductor electrodeposition. Elucidation of the deposition mechanism continues to remain

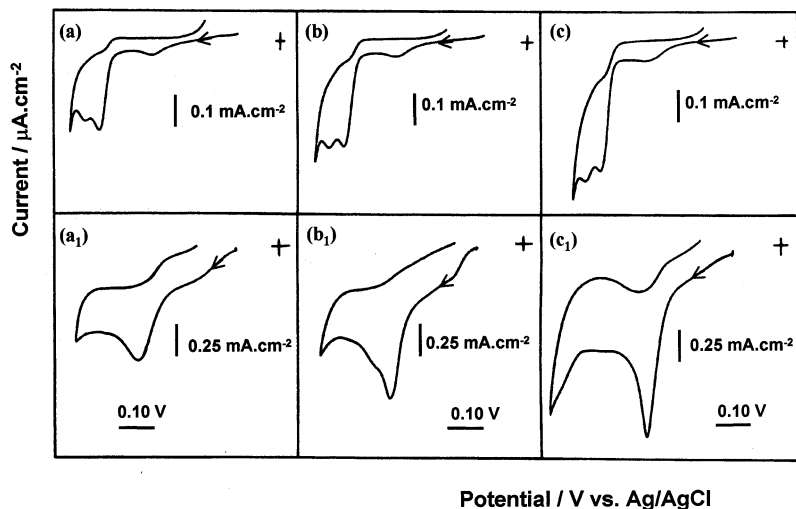


Fig. 6. Frames (a), (b), and (c) show the cathodic stripping of sulfur layers grown respectively to 130, 260, and 460  $\mu\text{C}$  thickness on the polycrystalline Au surface (as prescribed in Fig. 2, see text). The electrolyte was 0.1 M  $\text{Na}_2\text{SO}_4/0.05$  M  $\text{Na}_2\text{S}$  and the potential scan-rate was 20 mV/s. The voltammograms in frames (a<sub>1</sub>), (b<sub>1</sub>), and (c<sub>1</sub>) were the same electrodes as above but the sulfur stripping was done in a pH 2 0.01 M  $\text{In}_2(\text{SO}_4)_3$  electrolyte. The stripping of sulfur now proceeds concomitantly with the growth of  $\text{In}_2\text{S}_3$  layers (see Fig. 5).

an elusive goal in this system. The EQCM technique has been employed before, both by us and by other authors [19,23,49] for this purpose.

One interesting aspect of CdTe deposition is that the overall mechanism involves basically two successive electrochemical steps (the possibility of other parallel reactions also exist):



where the formation of CdTe takes place in Reaction 2b which can be considered as an underpotential deposition of cadmium in the presence of Te. To obtain stoichiometric CdTe it is usual to have Reaction 2a under diffusion control with low Te(IV) concentration, and to increase the rate of Reaction 2b by high cadmium concentration and as negative a deposition potential as possible. An elegant tool for investigating in situ the competition between the two reactions is to manipulate the hydrodynamic regime since virtually only Reaction 2a is affected.

Fig. 7 shows combined voltammetric and gravimetric measurements made under well-defined hydrodynamic condition by using rotating EQCM. We clearly see on the voltammogram characteristic electrochemical features of the CdTe system. The deposition of CdTe/Te films is associated with the presence of well-defined reduction waves between  $-0.20$  and  $-0.65$  V (vs. SCE). Many pieces of information can be extracted from such curves. As an example, the difference between the amplitude of the deposition current between

forward and back potential excursions is a striking point to study. Combining the quantity of electricity with the mass variation it appears that during the cathodic scan mostly tellurium is formed whereas during the reverse anodic sweep predominantly cadmium telluride tends to be formed. This can be associated with changes in the nature of the substrate: during the forward scan, the substrate is pristine gold but during the reverse scan the substrate is composed of both tellurium and cadmium formed below  $-0.66$  V versus SCE. Because of rather different work functions, cadmium provides an ohmic contact for the growth of

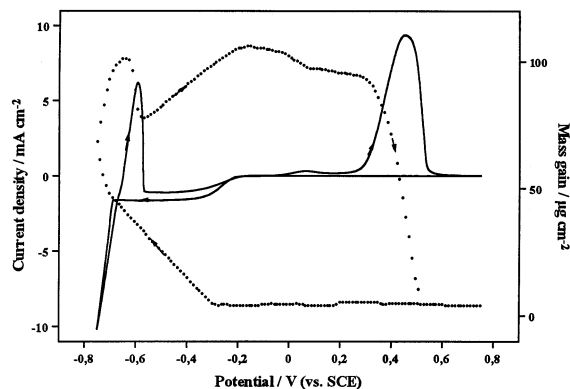


Fig. 7. Combined cyclic voltammetry (solid line) and EQCM (dotted line) data using a rotated EQCM set-up (electrode rotation speed = 200 RPM). The potential scan-rate was 5 mV/s and the bath conditions were as follows:  $T = 70^\circ\text{C}$ ,  $[\text{Te(IV)}] = 10^{-3}$  M,  $[\text{Cd(II)}] = 0.5$  M,  $\text{pH} = 1.4$ .

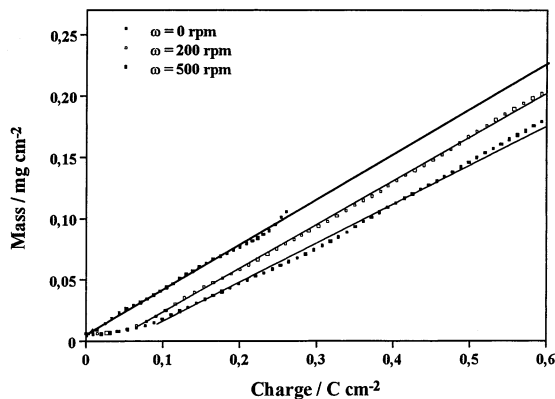


Fig. 8. Plots of charge versus mass for a set of films grown at  $-0.6$  V (vs. SCE). The parameter is the electrode rotation speed.

n-type CdTe, which is not the case for gold, promoting the deposition of Te to the detriment of CdTe. This illustrates the possibility of using EQCM to analyze the ohmicity of the substrate/layer interface which is very important for thin film applications.

Finally, Fig. 8 contains mass versus charge plots obtained at a constant deposition potential ( $-0.6$  V vs. SCE). These data illustrate the virtue of combining QCM with coulometry experiments. Three sets of data are shown at variant hydrodynamic conditions (0, 200, and 500 RPM) corresponding to current densities of 0.3, 1.2 and  $2.15 \text{ mA cm}^{-2}$ , respectively. The decrease of the slope is related to the enrichment in elemental tellurium, relative to the result at 0 RPM where the deposit should be close to stoichiometry (as deduced from EDX measurements). The excess of Te, deduced from the experimental slopes with respect to the value for 0 RPM is 20% at 200 RPM and 40% at 500 RPM. These conditions illustrate the case of a boundary kinetic regime between Reactions 2a and 2b above and, more generally, how EQCM can be useful for gaining compositional insights. A systematic study of these aspects, including the influence of deposition potential is in progress.

### Acknowledgements

D.L. and C.L. acknowledge support from the European Union (Program No. JOR 3-CT-97-0150). N.R. de T and K.R. thank the US Department of Energy (Division of Basic Energy Sciences) for partial financial support of this research. Last, but not least, we thank Gloria Madden for assistance in the preparation of this manuscript.

### References

- [1] G. Sauerbrey, *Z. Phys.* 155 (1959) 206.
- [2] R. Schumacher, *Angew Chem.* 29 (1990) 329.
- [3] D.A. Buttry, *Electroanal. Chem.* 17 (1991) 1.
- [4] K.K. Kanazawa, O.R. Melroy, *IBM J. Res. Devel.* 37 (1993) 157.
- [5] K. Doblhofer, K. Rajeshwar, in: T.A. Skotheim, R.L. Elsenbaumer, J.R. Reynolds (Eds.) *Handbook of Conducting Polymers*, second ed., Marcel Dekker, New York, 1998, p. 531 (Review).
- [6] G. Hodes, in: I. Rubinstein (Ed.), *Physical Electrochemistry*, Marcel Dekker, New York, 1995, p. 515 (Chapter 11).
- [7] K. Rajeshwar, *Adv. Mater.* 4 (1992) 23.
- [8] S. Gorer, G. Hodes, in: P.V. Kamat, D. Meisel (Eds.), *Semiconductor Nanoclusters — Physical, Chemical, and Catalytic Aspects*, Elsevier, Amsterdam, 1997, p. 297.
- [9] D. Lincot, M. Froment, H. Cachet, *Adv. Electrochem. Sci. Eng.* 6 (1999) 165.
- [10] K. Rajeshwar, N.R. de Tacconi, in: P.V. Kamat, D. Meisel (Eds.), *Semiconductor Nanoclusters — Physical, Chemical, and Catalytic Aspects*, Elsevier, Amsterdam, 1997, p. 321.
- [11] N.R. de Tacconi, O. Medvedko, K. Rajeshwar, *J. Electroanal. Chem.* 379 (1994) 545.
- [12] N.R. de Tacconi, K. Rajeshwar, *J. Electroanal. Chem.* 444 (1998) 7.
- [13] N. Myung, N.R. de Tacconi, K. Rajeshwar, *Electrochem. Commun.* 1 (1999) 42.
- [14] T.D. Golden, M.G. Shumsky, Y. Zhou, et al., *Chem. Mater.* 8 (1996) 2499.
- [15] S. Peulon, D. Lincot, *Adv. Mater.* 8 (1996) 166.
- [16] S. Peulon, D. Lincot, *J. Electrochem. Soc.* 145 (1998) 864.
- [17] Z.H. Gu, T.Z. Fahidy, *J. Electrochem. Soc.* 146 (1999) 156.
- [18] J.A. Switzer, *Am. Ceram. Bull.* 66 (1987) 1521.
- [19] E. Mori, C.K. Baker, J.R. Reynolds, et al., *J. Electroanal. Chem.* 252 (1988) 441.
- [20] C. Wei, C.S.C. Bose, K. Rajeshwar, *J. Electroanal. Chem.* 327 (1992) 331.
- [21] N. Myung, C. Wei, K. Rajeshwar, *J. Electroanal. Chem.* 356 (1993) 281.
- [22] N. Myung, J.H. Jun, H.B. Ku, *Microchem. J.* 62 (1999) 15.
- [23] C. Wei, N. Myung, K. Rajeshwar, *J. Electroanal. Chem.* 347 (1993) 223.
- [24] N.R. de Tacconi, K. Rajeshwar, R.O. Lezna, *J. Phys. Chem.* 100 (1996) 18234.
- [25] M.I. Schimmel, N.R. de Tacconi, K. Rajeshwar, *J. Electroanal. Chem.* 453 (1998) 187.
- [26] A. Marlot, J. Vedel, *J. Electrochem. Soc.* 146 (1999) 177.
- [27] E.W. Bohannon, L.-Y. Huang, F.S. Miller, et al., *Langmuir* 15 (1999) 813.
- [28] D. Lincot, R. Ortega-Borges, *J. Electrochem. Soc.* 139 (1880) 1992.
- [29] R. Ortega-Borges, D. Lincot, *J. Electrochem. Soc.* 140 (1993) 3464.
- [30] B. Mokili, M. Froment, D. Lincot, *J. Phys. Chem.* 99 (1995) 26.

- [31] H. Cachet, M. Froment, G. Maurin, *J. Electroanal. Chem.* 406 (1996) 239.
- [32] H. Cachet, H. Essaaidi, M. Froment, et al., *J. Electroanal. Chem.* 396 (1995) 75.
- [33] C. Wei, K. Rajeshwar, *J. Electroanal. Chem.* 375 (1994) 109.
- [34] C.S.C. Bose, K. Rajeshwar, *J. Electroanal. Chem.* 333 (1992) 235.
- [35] A.N. Buckley, I.C. Hamilton, R. Woods, *J. Electroanal. Chem.* 216 (1987) 213.
- [36] R.O. Lezna, N.R. de Tacconi, A.J. Arvia, *J. Electroanal. Chem.* 283 (1990) 319.
- [37] X. Gao, Y. Zhang, M.J. Weaver, *Langmuir* 8 (1992) 668.
- [38] L.P. Colletti, D. Teklay, J.L. Stickney, *J. Electroanal. Chem.* 369 (1994) 145.
- [39] B. Miller, A. Heller, *Nature* 262 (1967) 680.
- [40] L.M. Peter, *Electrochim. Acta* 23 (1978) 165.
- [41] L.-S.R. Yeh, P.G. Hudson, A. Damjanovic, *J. Appl. Electrochem.* 12 (1982) 153.
- [42] V.I. Birss, L.E. Kee, *J. Electrochem. Soc.* 133 (1986) 2097.
- [43] S.B. Saidman, J.R. Vilche, A.J. Arvia, *Electrochim. Acta* 32 (1987) 1153.
- [44] M. Krebs, M.I. Sosa, K.E. Heusler, *J. Electroanal. Chem.* 301 (1991) 101.
- [45] D. Ham, K.K. Mishra, K. Rajeshwar, *J. Electrochem. Soc.* 138 (1991) 100.
- [46] N.R. de Tacconi, K. Rajeshwar, *J. Phys. Chem.* 97 (1993) 6504.
- [47] M.P.R. Panicker, M. Knaster, F.A. Kröger, *J. Electrochem. Soc.* 125 (1978) 566.
- [48] F.A. Kröger, *J. Electrochem. Soc.* 125 (1978) 2028.
- [49] J.G.N. Matias, J.F. Juliao, D.M. Soares, et al., *J. Electroanal. Chem.* 431 (1997) 163.